


# Nonreciprocal electronic transport in PdCrO<sub>2</sub>: Implication of spatial inversion symmetry breaking

M. Akaike,<sup>1</sup> Y. Nii,<sup>1,2</sup> H. Masuda,<sup>1</sup> and Y. Onose<sup>1</sup>

<sup>1</sup>*Institute for Materials Research, Tohoku University, Sendai 980-8577, Japan*

<sup>2</sup>*PRESTO, Japan Science and Technology Agency (JST), Kawaguchi 332-0012, Japan*

 (Received 2 December 2020; revised 18 March 2021; accepted 19 May 2021; published 28 May 2021)

Noncollinear spin structures, such as helimagnetic structures, have been gathering attention because of their nontrivial magnetic transport induced by topological effects. For a precise determination of spin structure, in addition to traditional neutron diffraction measurements, the time-reversal-odd rectification of electronic transport, which is referred to as nonreciprocal electronic transport, provides useful information because of the symmetry sensitivity. We observed nonreciprocal electronic transport below the Néel temperature in an itinerant antiferromagnet, PdCrO<sub>2</sub>, with a 120° spin structure. This implies breaking of spatial inversion symmetry owing to the magnetic ordering. Possible spin structures are discussed based on the magnetic field dependence of nonreciprocal transport.

DOI: [10.1103/PhysRevB.103.184428](https://doi.org/10.1103/PhysRevB.103.184428)

## I. INTRODUCTION

Noncollinear spin structures frequently give rise to unusual magnetotransport properties. For example, the fictitious field originating from scalar spin chirality deflects an electric current, giving rise to the unusual magnetic field dependence of Hall conductivity [1]. To explore the mechanisms of such properties, an accurate determination of magnetic structure is essential. While neutron scattering measurements are the most powerful method for determining magnetic order, other experimental probes sensitive to the magnetic symmetry also provide valuable information and are promising for further refinement. In particular, the second-harmonic generation (SHG) of light has played a significant role in the identification of noncentrosymmetric magnetic structures [2,3].

Another class of symmetry sensitive probes is nonreciprocal unidirectional responses [4,5]. When spatial inversion and time-reversal symmetries are simultaneously broken in some materials, the response to a stimulus moving along a direction become different from that to reversely moving one. In the case of electronic transport, Rikken and coworkers first showed that the nonreciprocity can be deduced by the substitution of current  $I$  for the wave vector  $k$  in the expansion of diagonal conductivity based on the Onsager's relation [6]

$$\begin{aligned} \sigma(k, H) &= \sigma(0, 0) + \alpha kH + \dots \\ \rightarrow \sigma(I, H) &= \sigma(0, 0) + \alpha IH + \dots \end{aligned} \quad (1)$$

Here,  $\sigma(k, H)$  is an electrical conductivity at  $k$  and magnetic field  $H$ , and  $\alpha$  is a proportionality constant. They suggested that  $\alpha$  should be nonzero for chiral materials and its sign dependent on the chirality, and experimentally demonstrated these features for a macroscopically twisted object. Subsequently, nonreciprocal electronic transport under magnetic field has been reported for several materials with noncentrosymmetric crystal structure such as BiTeBr, MnSi, and Te [7–9]. In CrNb<sub>3</sub>Se<sub>6</sub>, the nonreciprocal electronic trans-

port was observed to be considerably enhanced below the helimagnetic ordering temperature [10]. Quite recently, Jiang *et al.* showed that the magnetic breaking of spatial inversion symmetry can also induce the nonreciprocal electronic transport in a magnetic field for a helimagnet MnP with centrosymmetric crystal structure [11]. In general, for symmetry broken materials, the resistivity  $\rho$  depends on the sign of the electric current as follows:

$$\rho = \rho_1 + \rho_2 j, \quad (2)$$

where  $j$  is the electric current density and  $\rho_1$  and  $\rho_2$  are constant tensors. Either the time-reversal or spatial inversion operation changes the sign of  $\rho_2$ . In this case, the electric field  $E$  is expressed as

$$E = \rho_1 j + \rho_2 j^2. \quad (3)$$

This equation suggests that the nonreciprocal electronic transport can be viewed as the transport version of SHG. Similarly to the optical case, the tensor  $\rho_2$  is quite sensitive to the magnetic symmetry [2]. Therefore, it should be useful for probing noncentrosymmetric magnetic structures.

In the present work, we study the magnetic structure of the itinerant noncollinear antiferromagnet PdCrO<sub>2</sub> in terms of nonreciprocal electronic transport. We show the crystal and magnetic structures of PdCrO<sub>2</sub> in Fig. 1(a). PdCrO<sub>2</sub> has a centrosymmetric delafossite crystal structure consisting of Pd and Cr triangular lattices and interstitial oxygen. Below the antiferromagnetic transition temperature  $T_N = 37$  K, Cr magnetic moments show so-called 120° antiferromagnetic order in a plane parallel to the  $c$ -axis [12,13]. The nonlinear anomalous Hall effect emerges below approximately 20 K. Its origin was proposed to be the spin chirality mechanism [14–16]. While a recent neutron diffraction measurement suggests staggered stacking of 120° magnetic structures with different chiralities [13], further refinement seems useful for examining the unconven-

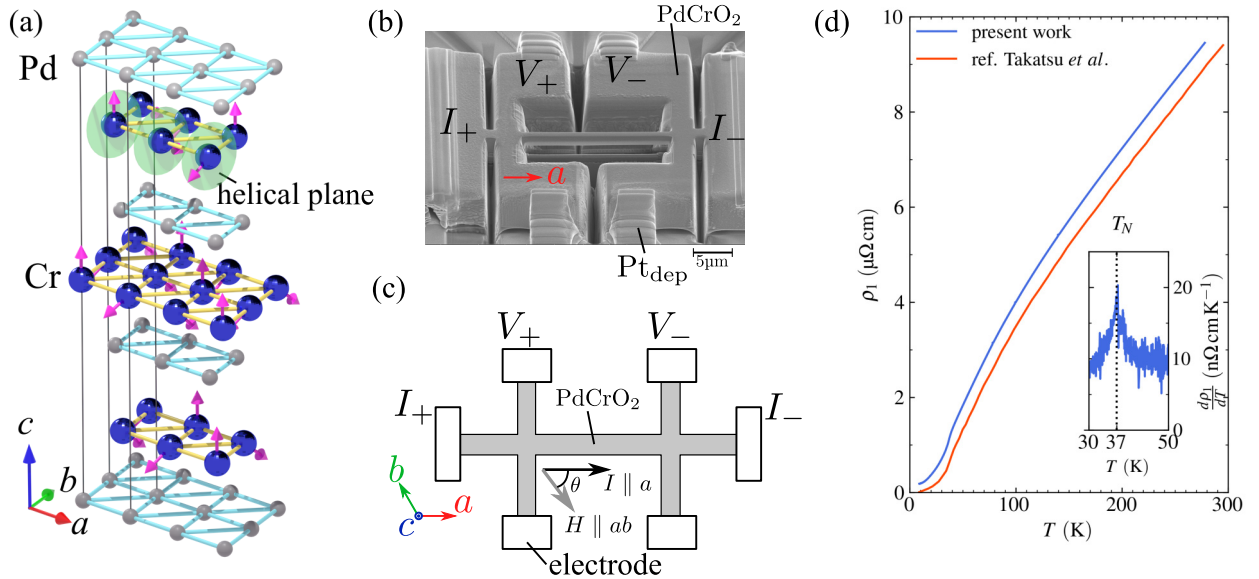


FIG. 1. (a) Crystal and magnetic structure of  $\text{PdCrO}_2$ . Large and small spheres show Cr and Pd atoms, respectively. Oxygen is not shown for clarity. Arrows on Cr atoms represent one possible  $120^\circ$  magnetic structure [model 1 shown in Fig. 6(d)]. Transparent circles stand for the helical planes. (b) Scanning electron microscope (SEM) image of the sample device. The device was sculpted out of a single crystal using a focused ion beam (FIB). Electrical contacts between the sample and electrodes were made from FIB-deposited Pt ( $\text{Pt}_{\text{dep}}$ ). (c) Top view of the device structure and experimental setup. The electric current is along the  $a$ -axis of the crystal. The  $c$ -axis is orthogonal to the device plane. (d) Temperature dependence of the electrical resistivity. The data reported by Takatsu *et al.* [17] is reproduced for comparison. Inset shows the derivative of resistivity for the present sample.

tional magnetic transport in this system. Here, we observed finite nonreciprocal electronic transport below the Néel temperature, implying breaking of spatial inversion symmetry due to magnetic order. Possible magnetic structures are discussed based on the magnetic field angle dependence of nonreciprocal electronic transport.

## II. EXPERIMENT

We grew single crystals of  $\text{PdCrO}_2$  utilizing the flux method. The details were almost the same as those reported in the literature [17]. For the precise measurement of nonreciprocal electronic transport, large electric current density is needed. For this purpose we extracted a small rectangular piece from a single crystal and microfabricated it by using focused ion beam (FIB) techniques [18]. To obtain larger electric current densities, the sample cross section was further reduced, as shown in Figs. 1(b) and 1(c). We measured the linear resistivity and nonreciprocal electronic transport with the standard four-probe method in a superconducting magnet. An AC electric current was applied along the thin rectangular bar with approximately  $1.0 \times 1.85 \mu\text{m}^2$  cross-sectional area, which was parallel to the crystal  $a$ -axis. We measured the first and second harmonic voltages between upper or lower pairs of electrodes with a distance of  $20 \mu\text{m}$  by using a lock-in amplifier with a frequency of 11.15 Hz. According to Eq. (3), the second harmonic signal corresponded to the nonreciprocal electronic transport, while the first one corresponded to ordinary resistivity [7]. The sample device was rotated in the superconducting magnet so that magnetic fields were applied along various in-plane crystal axes.

Figure 1(d) shows the temperature dependence of linear resistivity for the fabricated device. The amplitude of the applied current density was  $5.4 \times 10^7 \text{ A/m}^2$ , which was much smaller than that in the measurement of nonreciprocal electronic transport. The linear resistivity exhibited metallic temperature dependence and a kink around  $T_N$ . While the residual resistivity was larger than that in the previous report [17], the temperature dependence was almost the same. The inset shows the derivative of resistivity. A clear peak was discerned at  $T_N = 37 \text{ K}$ , which also coincides with the previous report [17]. These observations indicate that the sample degradation due to the FIB fabrication was minimal. In the measurement of nonreciprocal electronic transport, the sample resistance was used for estimating the sample temperature, taking the effect of Joule heating into account.

## III. RESULTS AND DISCUSSION

Before discussing the nonreciprocal electronic transport, let us discuss the temperature and magnetic field dependence of magnetoresistance to study the nature of magnetotransport in this system. Figure 2 shows the magnetoresistance  $\Delta\rho_1/\rho_1 = [\rho_1(H) - \rho_1(0)]/\rho_1(0)$  below 51 K for  $H \perp j$  and  $H \parallel j$ . For both configurations,  $\Delta\rho_1/\rho_1$  increased with temperature below around 30 K and decreased in the higher temperature range. The magnitude for the  $H \perp j$  case was much larger than that for the  $H \parallel j$  case. Figures 3(a) and 3(b), respectively, show the temperature dependence of  $\Delta\rho_1/\rho_1$  at respective magnetic fields for  $H \parallel j$  and  $H \perp j$ . For  $H \parallel j$ ,  $\Delta\rho_1/\rho_1$  showed a broad maximum around  $T_N$ , while the maximum temperature was lower for  $H \perp j$ .  $\Delta\rho_1/\rho_1$  for both configurations seemed to vanish when the tempera-

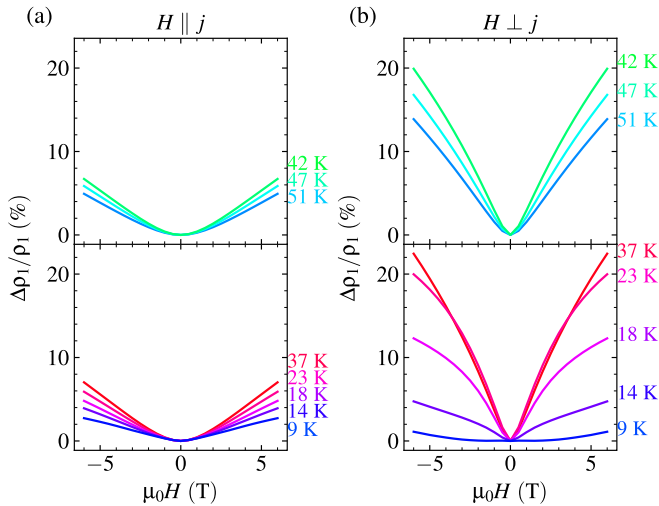


FIG. 2. Magnetic field dependence of the magnetoresistance  $\Delta\rho_1/\rho_1$  in (a)  $H \parallel j$  and (b)  $H \perp j$ .

ture approached 0 K. Above the maximum temperature, the decrease was quite gradual. These temperature dependencies suggest the relation to the antiferromagnetism. The anisotropy of magnetoresistance is relatively large in this material. In conventional metals, such anisotropy may be caused by the difference of carrier dynamics parallel and perpendicular to a magnetic field; the magnetic field deflects carriers moving along the perpendicular direction owing to the Lorentz force, but does not have the same result on those moving along the field. If this is the case, the magnetoresistance should become larger as the scattering rate or resistivity is decreased following the so-called Kohler's rule [19]. Nevertheless, in the present case, as the temperature is decreased below 30 K, the resistivity decreases and the magnetoresistance also decreases. Therefore, we cannot ascribe the origin of

anisotropy to the Lorentz force. Hence, we ascribed the origin to the modification of anisotropic magnetic structure in the magnetic field. When the magnetic field is applied, the magnetic moments are tilted to the field direction, and the Zeeman energy is reduced. The Zeeman energy gain is maximum when the helical plane is perpendicular to the magnetic field. Therefore, the helical plane tends to rotate in a magnetic field so as to be perpendicular to the magnetic field. Such helical plane rotations are generally observed in helimagnets [20,21]. In PdCrO<sub>2</sub>, studies of neutron diffraction and magnetic torque probed the magnetic transition relevant to the helical plane rotation at around 7 T below 1.5 K [22]. At higher temperature, the helical plane rotation should emerge in the lower field region, but the transition signature may be smeared out because the in-plane anisotropy is smaller than the thermal energy [23]. The strong anisotropy of magnetoresistance seems to be reflected in the difference of resistivities parallel and perpendicular to the helical plane. In fact, the temperature dependence of magnetoresistance seems to be reflected by the evolution of antiferromagnetic correlation. The possible origins of magnetoresistance are spin scattering and magnon scattering. In the first case, the incomplete magnetic ordering scatters the carriers and magnons do in the second case. In any case, the magnetoresistance should increase with decreasing temperature in the high temperature region above  $T_N$  owing to the evolution of antiferromagnetic correlation, and decrease toward the lowest temperature because of either the completion of antiferromagnetic ordering or the dominance of elastic scattering.

Next, let us move on to the nonreciprocal electronic transport. We measured the second harmonic resistivity with a current density of  $1.0 \times 10^9$  A/m<sup>2</sup> to study the nonreciprocal electronic transport. According to previous works [5,6], the component of second harmonic resistivity showing antisymmetric magnetic field dependence corresponds to the nonreciprocal electronic transport, while the symmetric component includes extrinsic effects such as problems related to the electrical contacts. To extract the intrinsic component, we antisymmetrize the second harmonic resistivity as

$$\rho_{\text{asym}}^{2\omega} = [\rho^{2\omega}(H) - \rho^{2\omega}(-H)]/2, \quad (4)$$

where  $\rho^{2\omega}$  is the second harmonic resistivity. Figure 4(a) shows the magnetic field dependence of nonreciprocal electronic resistivity  $\rho_{\text{asym}}^{2\omega}$  at various temperatures for  $H \parallel j$  and  $H \perp j$ . While the nonreciprocal signal was hardly observed above  $T_N$  for both configurations, noticeable signals began to grow with decreasing temperature from  $T_N$ . For  $H \parallel j$ , a positive signal increased in the high field region. At low temperatures, linear-like field dependence was observed. On the other hand, a step-like positive signal was discerned below  $T_N$  for  $H \perp j$ . At low temperatures, negative linear field dependence appeared. To discuss the temperature dependence in more detail, we plot the average of  $\rho_{\text{asym}}^{2\omega}$  between 4.5 T and 6 T for  $H \parallel j$ , and that between 0.5 T and 2 T for  $H \perp j$  as functions of temperature in Figs. 4(b) and 4(c). It is clear from these figures that nonreciprocal electronic transport evolves rapidly below  $T_N$ . This implies that the magnetic order broke the spatial inversion symmetry. Nevertheless, we have to note that a small but nonzero signal was observed above  $T_N$ , although the crystal structure is reported to be centrosymmetric.

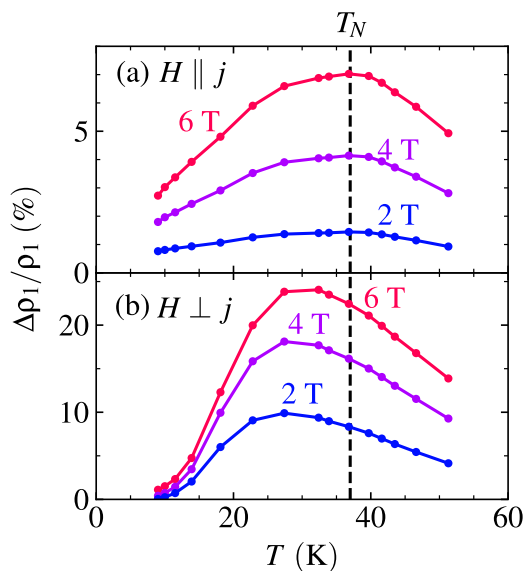


FIG. 3. (a,b) Temperature dependence of magnetoresistance  $\Delta\rho_1/\rho_1$  in (a)  $H \parallel j$  and (b)  $H \perp j$ . The vertical dashed line represents the Néel temperature.

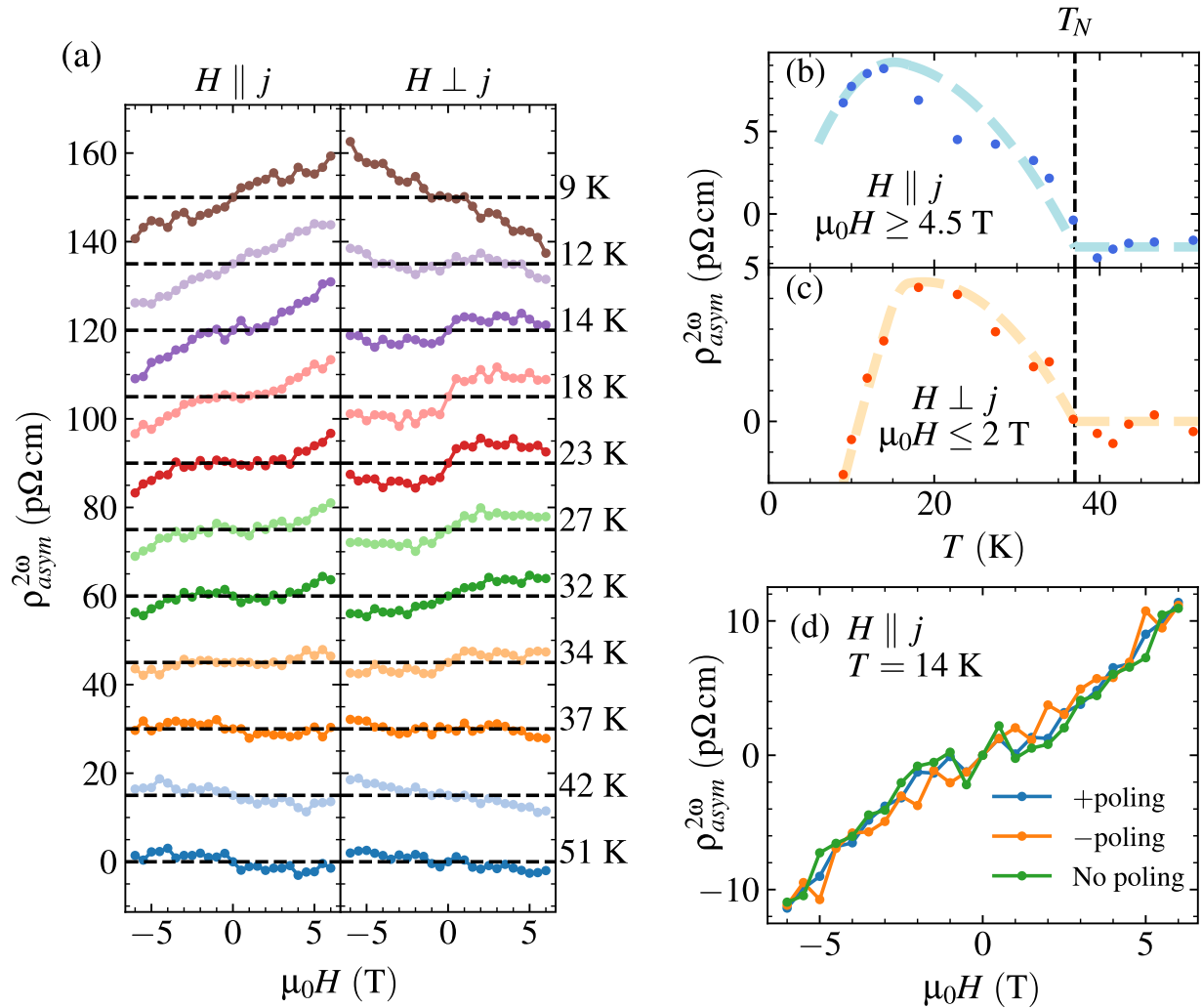


FIG. 4. (a) Magnetic field dependence of the nonreciprocal electronic resistivity  $\rho_{\text{asym}}^{2\omega}$  at various temperatures for  $H \parallel j$  and  $H \perp j$ . While the negative field data obtained by Eq. (4) are merely the copy of the positive field data, we also plot the data at negative fields just for clarity of the figure. Vertical offsets are added also for the clarity. The dashed lines represent the zero levels. (b,c) Temperature dependence of the averaged nonreciprocal electrical resistivities in (b)  $H \parallel j$  and (c)  $H \perp j$ . For  $H \parallel j$ , the data above 4.5 T are averaged, while the averaged region is  $0.5 \text{ T} \leq H \leq 2 \text{ T}$  for  $H \perp j$ . The vertical thin dashed line represents the Néel temperature. The thick dashed lines are merely guides for the eyes. (d)  $\rho_{\text{asym}}^{2\omega}$  at 14 K after the phase transition with the application of parallel magnetic field  $H$  and electric current  $j$  (+poling), that after the transition with antiparallel  $H$  and  $j$  (-poling), and that after the transition without  $H$  and  $j$  (no poling).

Perhaps symmetry breaking at the contacts or edges of the sample caused the extrinsic voltages. Around 15 K,  $\rho_{\text{asym}}^{2\omega}$  for both the configurations begins to decrease with decreasing temperature. Because the magnetoresistance is suppressed in this temperature range, the change of transport characteristics may cause the temperature change. Another point that we have to take into account is the effect of magnetic domains. In general, when the inversion symmetry is broken at the magnetic ordering temperature, there should be magnetic domains that are converted to each other by the spatial inversion operation. The example is shown in Appendix B. The equally distributed domains should cancel the nonreciprocal electronic transport signal. In reality, we observed a finite signal below  $T_N$ , indicating unequal volumes of these magnetic domains. Jiang *et al.* [11] controlled the helicity domain of the helical spin structure in MnP by means of the simultaneous application of the magnetic field and electric current in the course of

the magnetic transition. We also tried to control the magnetic domain with a magnetic field and DC electric current. Figure 4(d) shows  $\rho_{\text{asym}}^{2\omega}$  at 14 K for  $H \parallel j$  after the magnetic transition with a magnetic field of 6 T and electric current density of  $3.2 \times 10^9 \text{ A/m}^2$ , together with that after the magnetic transition without any external stimuli. As clearly shown in the figure, the nonreciprocal transport signal was not affected by the application of a magnetic field and electric current in the course of the phase transition. Therefore, the domain volumes ratio relevant to the spatial inversion symmetry seems fixed by some effects such as stress, and cannot be controlled by the external fields [24]. While the sign and magnitude of nonreciprocal electronic transport may depend on the samples in this case, the temperature and magnetic field dependencies should be reproducible.

To understand the magnetic symmetry in more detail, we investigated the magnetic field angle dependence of



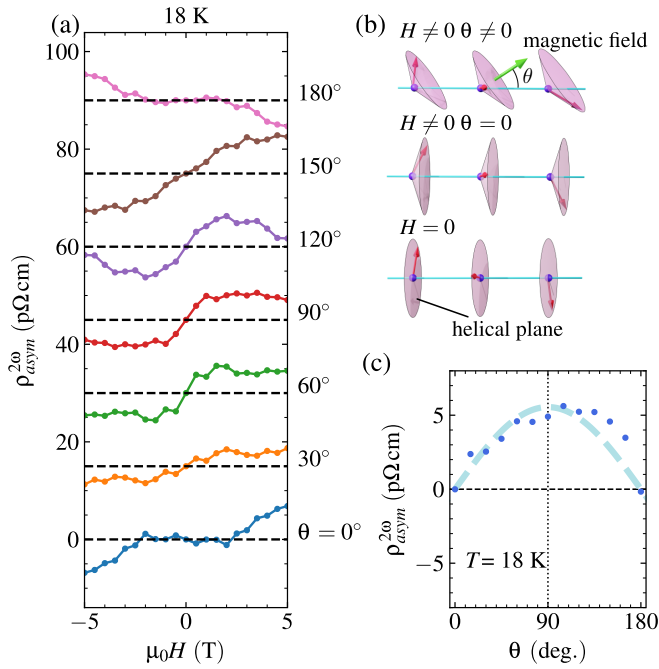


FIG. 5. (a) Nonreciprocal electronic resistivity at 18 K as a function of magnetic field with various angles  $\theta$ . The sign definition of  $\theta$  is shown in Fig. 1(c). Vertical offsets are added for clarity. The dashed lines represent the zero levels. (b) Image of helical plane rotation in a tilted magnetic field. (c) Angle dependence of nonreciprocal electronic resistivity averaged in the magnetic field range of 0.5 T  $\leq H \leq 2$  T at 18 K.

nonreciprocal electronic transport. Figure 5(a) shows the nonreciprocal electronic transport at 18 K as a function of magnetic fields in various directions. When the magnetic field was perpendicular to the electric current, a step-like increase of the nonreciprocal electronic transport was observed. The magnitude of the step gradually decreased as the magnetic field direction became closer to that of the electric current. Figure 5(c) shows the average of nonreciprocal electronic transport at 18 K between 0.5 T and 2 T as a function of the magnetic field angle, showing  $\sin \theta$ -like angle dependence. As mentioned above, the helical plane is readily rotated in a magnetic field so as to be perpendicular to the magnetic field, as shown in Fig. 5(b). Therefore, the magnetic field angle can be viewed as the angle of the helical plane.

Then let us discuss possible spin structures based on the magnetic field dependence. From a previous report on a neutron diffraction experiment [12,13], it is quite certain that a  $120^\circ$  spin structure is realized at zero magnetic field. The chirality of the  $120^\circ$  structure in a Cr layer is opposite to those in neighboring layers [13]. Namely, two layers of  $120^\circ$  spin structures with different signs of chirality are alternately stacked along the  $c$ -axis. Hereafter, we discuss the nonreciprocal electronic transport in the alternating-chirality magnetic structures that are consistent with the neutron diffraction experiment and  $R\bar{3}m$  symmetry [13] (see Appendix C). The simplest structure with alternating chirality is shown in Fig. 6(c). In this case, the spin angles of three sublattices of  $120^\circ$  spin structures are the same for each layer, but the order of the three angles is different:  $S_1, S_2, S_3, S_1, \dots$ ,

for odd layers and  $S_1, S_3, S_2, S_1, \dots$ , for even layers. When the helical plane is perpendicular to the  $a$ -axis, the magnetic point group is  $2'/m'$ , which is the centrosymmetric one and nonreciprocal transport should vanish. In this crystal structure, there are two other axes equivalent to the  $a$ -axis in the plane ( $\theta = 60^\circ$  and  $120^\circ$ ). Therefore, if this magnetic structure were realized, the nonreciprocal transport would be suppressed in the small magnetic field along these axes, which is different from the present observation. Figure 6(d) shows an alternating-chirality spin structure with lower symmetry. This is close to one of possible spin structures proposed by Takatsu *et al.* [13], but slightly modified so as to be expressed by two magnetic wave vectors  $(-2/3, 1/3, 0)$  and  $(1/3, -2/3, 1/2)$  (see Appendix C). In this case, the spin moments in the odd layers are not parallel to any moments in the even layers, while all the helical planes are parallel to each other. The magnetic point group becomes  $2'$  when the helical plane is perpendicular to the  $a$ -axis. In this magnetic symmetry, the spatial inversion and time-reversal symmetries are both broken, and therefore nonreciprocal electronic transport may emerge even at zero magnetic field. According to a symmetry analysis (Appendix A), the nonreciprocal transport is allowed when the electronic current is perpendicular to the principal axis of  $2'$  symmetry, which corresponds to the normal direction of the helical plane. In contrast, when the current is parallel to the principle axis, the nonreciprocal transport is forbidden. We here speculate that the observed step-like structure may be explained based on this symmetry. In this magnetic state, the magnetic structure after the time-reversal operation is discriminated from the original one (see Appendix B). Then, the signs of nonreciprocal transport for these two states should be opposite to each other. In a certain magnetic field, one of these two states is favored, and the other is favored in the reversed field. Therefore, the step-like feature of nonreciprocal transport around zero field is expected. When  $H$  is parallel to the  $\theta = 0^\circ$  direction, the helical plane is normal to the  $a$ -axis and, therefore, the nonreciprocal transport along the  $a$ -axis is forbidden. On the other hand, it is allowed at  $\theta = 60^\circ$  and  $120^\circ$ . The magnetic symmetry becomes lower but the extrapolated  $\theta$  dependence may be expected when the magnetic field is not parallel to the principle axes of the crystal structure. Thus, the observed  $\theta$  dependence can be qualitatively explained. Nevertheless, it is not certain at present and needs to be investigated how effectively domain control is achieved in a low magnetic field. In spite of the time-reversal symmetry breaking, the magnetic domains do not have net magnetization. The higher-order magnetic susceptibility couples to the magnetic field, but, at present, we are not so sure how effectively the magnetic field control the time-reversal symmetry. In Fig. 6(e), an even lower symmetry candidate of the spin structure is depicted. The neutron diffraction study suggests that this is the most plausible structure [13]. This is realized by alternating rotation around the  $c$ -axis of the spin structure shown in Fig. 6(d). In this case the magnetic point group is 1, irrespective of the helical plane angle. The magnetic field angle dependence of nonreciprocal transport cannot be explained, at least in terms of symmetry, based on this model. Our measurement suggests that symmetry lowering from model 2 should be small so that the nonreciprocal transport is suppressed at  $\theta = 0$ .

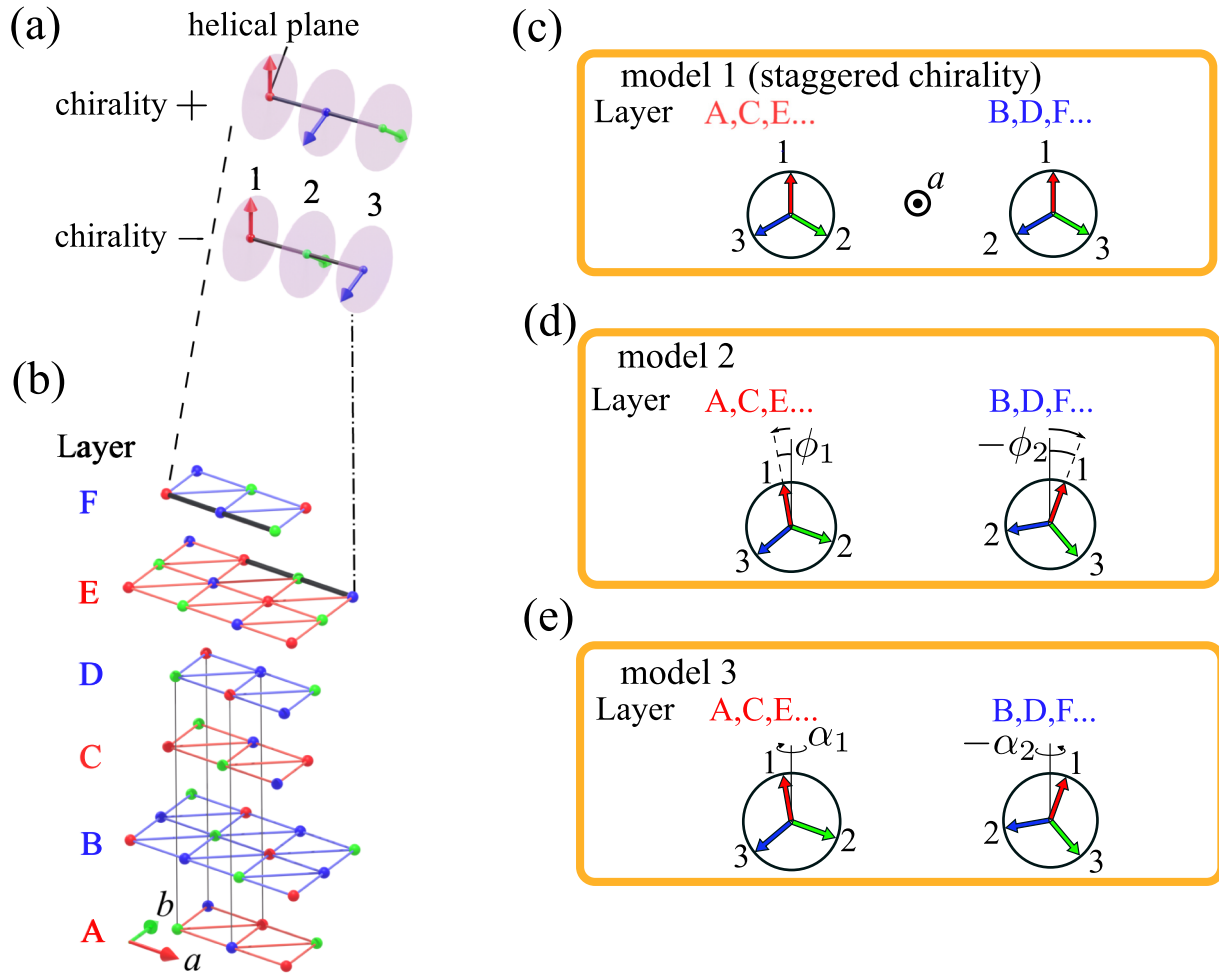


FIG. 6. (a) Image of the  $120^\circ$  spin structure and helical planes. The numbers 1, 2, 3 stand for the order of three cyclic spins along the  $a$ -axis. When two spins out of the three are exchanged, the chirality is reversed. Two chiral states are denoted as chirality + and chirality -. (b) Illustration of Cr magnetic layers. A, B, C, D, E, F, and so on are labels for the layers. The  $120^\circ$  spin structures in layers A, C, and E have chirality -, and those in layers B, D, and F have chirality +. (c) Illustration of simple  $120^\circ$  magnetic structure with staggered chirality (model 1). Odd layers and even layers have opposite chirality, but helical planes are parallel to each other and the angles of the three spins are the same for all layers. (d) Illustration of lower-symmetry magnetic structure with staggered chirality (model 2). The angles of three spins for layers A, C, and E are different from those for layers B, D, and F. All the helical planes are parallel. (e) Illustration of even lower-symmetry magnetic structure with staggered chirality (model 3). The helical planes for layers A, C, and E are not parallel to those for B, D, and F in this case.

#### IV. CONCLUSION

In conclusion, we observed nonreciprocal electronic resistivity below  $T_N$ . This implied that the antiferromagnetic order breaks the spatial inversion symmetry. A possible  $120^\circ$  structure with alternating chirality was discussed based on the angular dependence of nonreciprocal transport while the complete understanding of magnetic field dependence was not achieved with this model at present. To our knowledge, there have been no previous studies of magnetic structures based on nonreciprocal electronic transport. The present result may pave the way to a new direction in magnetic symmetry research.

#### ACKNOWLEDGMENTS

The device was fabricated partly by the Collaborative Research and Development Center for Advanced Materials,

Tohoku University with the help of K. Takanashi and T. Seki. FIB fabrication of the device was performed in the Electron Microscopy Center, Tohoku University with the help of T. Konno and Y. Kodama. This work was supported, in part, by JSPS KAKENHI (Grants No. JP16H04008, No. JP17H05176, No. JP18K13494, No. JP20K03828, and No. JP21H01036), PRESTO (Grant No. JPMJPR19L6), the Mitsubishi Foundation, and the Murata Science Foundation.

#### APPENDIX A: SYMMETRY ANALYSIS OF NONRECIPROCAL ELECTRONIC TRANSPORT IN THE $2'$ MAGNETIC POINT-GROUP SYMMETRY

In the magnetic systems, the nonreciprocal electronic transport should strongly depend on the magnetic symmetry. For this reason, the magnetic field dependence does not follow a simple linear relation [10,11]. In the  $2'$  magnetic

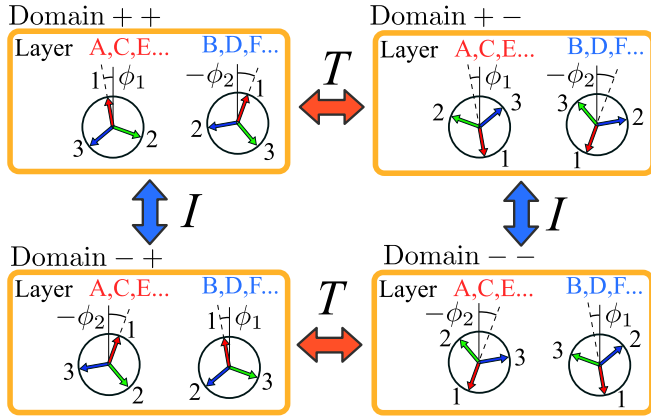


FIG. 7. Four magnetic domains of model 2 in Fig. 6(d). Domain  $-+$  and Domain  $+-$  are transformed by spatial inversion ( $I$ ) and time-reversal ( $T$ ) operations from Domain  $++$ , respectively. Domain  $--$  is by the combination of  $I$  and  $T$  operations.

point group symmetry, the magnetic structures before and after the time-reversal operation are discriminated from each other and the conductivity should also depend on which structure is realized. We labeled them as  $\eta = \pm 1$  and deduced the nonreciprocal electronic conductivity similarly to the Rikken's method mentioned above as

$$\begin{aligned} \sigma(k, \eta) &= \sigma + \alpha k \eta + \dots \\ \rightarrow \sigma(I, \eta) &= \sigma + \alpha I \eta + \dots \end{aligned} \quad (\text{A1})$$

The second term seems to correspond to the spontaneous nonreciprocal electronic transport. When the electric current is parallel to the principle axis of  $2'$  symmetry,  $180^\circ$  rotation of the system around the current direction does not change the conductivity, but  $\eta$  should be reversed. Thus, the nonreciprocal electronic transport vanishes when the current is parallel to the principle axis. If it is not parallel, there is no relation that forbids the nonreciprocal transport. While Neumann's Principle for space-time symmetry cannot be applied to transport properties, the selection rule obtained above is similar to that based on Neumann's Principle [25].

## APPENDIX B: MAGNETIC DOMAINS FOR MODEL 2

In this system, there are many possible magnetic domains. As examples, we show the possible magnetic domains in the model 2. In this case, there are three equivalent helical plane directions. For each helical plane direction, there are four magnetic domains. As shown in Fig. 7, the time-reversal or spatial inversion operation transforms one into another.

## APPENDIX C: TWO WAVE VECTORS' DESCRIPTION OF MAGNETIC MODELS

Based on the neutron diffraction experiment and  $R\bar{3}m$  space group symmetry, Takatsu *et al.* showed that a magnetic domain should be expressed with two wave vectors  $\mathbf{q}_1 = (-2/3, 1/3, 0)$  and  $\mathbf{q}_2 = (1/3, -2/3, 1/2)$  [13]. Here

we confirm that our spin models satisfy the constraint. In model 3, spins at 1, 2, 3 Cr sites for A, C, E layers are

$$\begin{aligned} \mathbf{S}_{A1} &= \cos \phi_1 \mathbf{e}_z - \cos \alpha_1 \sin \phi_1 \mathbf{e}_y \\ &\quad - \sin \alpha_1 \sin \phi_1 \mathbf{e}_x, \end{aligned} \quad (\text{C1})$$

$$\begin{aligned} \mathbf{S}_{A2} &= \cos(\phi_1 - 2/3\pi) \mathbf{e}_z - \cos \alpha_1 \sin(\phi_1 - 2/3\pi) \mathbf{e}_y \\ &\quad - \sin \alpha_1 \sin(\phi_1 - 2/3\pi) \mathbf{e}_x, \end{aligned} \quad (\text{C2})$$

$$\begin{aligned} \mathbf{S}_{A3} &= \cos(\phi_1 + 2/3\pi) \mathbf{e}_z - \cos \alpha_1 \sin(\phi_1 + 2/3\pi) \mathbf{e}_y \\ &\quad - \sin \alpha_1 \sin(\phi_1 + 2/3\pi) \mathbf{e}_x. \end{aligned} \quad (\text{C3})$$

Spins for B, D, F layers are

$$\begin{aligned} \mathbf{S}_{B1} &= \cos \phi_2 \mathbf{e}_z + \cos \alpha_2 \sin \phi_2 \mathbf{e}_y \\ &\quad - \sin \alpha_2 \sin \phi_2 \mathbf{e}_x, \end{aligned} \quad (\text{C4})$$

$$\begin{aligned} \mathbf{S}_{B2} &= \cos(\phi_2 - 2/3\pi) \mathbf{e}_z + \cos \alpha_2 \sin(\phi_2 - 2/3\pi) \mathbf{e}_y \\ &\quad - \sin \alpha_2 \sin(\phi_2 - 2/3\pi) \mathbf{e}_x, \end{aligned} \quad (\text{C5})$$

$$\begin{aligned} \mathbf{S}_{B3} &= \cos(\phi_2 + 2/3\pi) \mathbf{e}_z + \cos \alpha_2 \sin(\phi_2 + 2/3\pi) \mathbf{e}_y \\ &\quad - \sin \alpha_2 \sin(\phi_2 + 2/3\pi) \mathbf{e}_x. \end{aligned} \quad (\text{C6})$$

Here,  $\mathbf{e}_x, \mathbf{e}_y, \mathbf{e}_z$  are the basis of a Cartesian coordinate system and  $\mathbf{e}_x \parallel (1, 0, 0)$  and  $\mathbf{e}_z \parallel (0, 0, 1)$ . By the Fourier transformation, these spins can be expressed as

$$\begin{aligned} \mathbf{S}(\mathbf{R}) &= \mathbf{S}_1 \cos(\mathbf{q}_1 \cdot \mathbf{R} - \phi_2) + \mathbf{S}_2 \sin(\mathbf{q}_1 \cdot \mathbf{R} - \phi_2) \\ &\quad + \mathbf{S}_3 \cos(\mathbf{q}_2 \cdot \mathbf{R} - \phi_2) + \mathbf{S}_4 \sin(\mathbf{q}_2 \cdot \mathbf{R} - \phi_2), \end{aligned} \quad (\text{C7})$$

where  $\mathbf{R}$  is the positions of 18 Cr spin moments in a unit cell

$$\begin{aligned} \mathbf{R}_{A1} &= (-2/3, -4/3, 1/6), \mathbf{R}_{B1} = (0, 0, 1/2), \\ \mathbf{R}_{C1} &= (-1/3, -2/3, 5/6), \mathbf{R}_{D1} = (-2/3, -4/3, 7/6), \\ \mathbf{R}_{E1} &= (0, 0, 3/2), \mathbf{R}_{F1} = (-1/3, -2/3, 11/6), \\ \mathbf{R}_{X2} &= \mathbf{R}_{X1} + (1, 0, 0), \\ \mathbf{R}_{X3} &= \mathbf{R}_{X1} + (2, 0, 0) \quad (X = A, B, C, \dots). \end{aligned} \quad (\text{C8})$$

The constant vectors  $\mathbf{S}_1, \mathbf{S}_2, \mathbf{S}_3, \mathbf{S}_4$  are

$$\begin{aligned} \mathbf{S}_1 &= \frac{S}{2} \{ [1 + \cos(\phi_1 - \phi_2)] \mathbf{e}_z - \cos \alpha_1 \sin(\phi_1 - \phi_2) \mathbf{e}_y \\ &\quad - \sin \alpha_1 \sin(\phi_1 - \phi_2) \mathbf{e}_x \}, \end{aligned} \quad (\text{C9})$$

$$\begin{aligned} \mathbf{S}_2 &= \frac{S}{2} \{ \sin(\phi_1 - \phi_2) \mathbf{e}_z + [\cos \alpha_1 \cos(\phi_1 - \phi_2) - \cos \alpha_2] \mathbf{e}_y \\ &\quad + [\sin \alpha_1 \cos(\phi_1 - \phi_2) + \sin \alpha_2] \mathbf{e}_x \}, \end{aligned} \quad (\text{C10})$$

$$\begin{aligned} \mathbf{S}_3 &= \frac{S}{2} \{ \sin(\phi_1 - \phi_2) \mathbf{e}_z + [\cos \alpha_1 \cos(\phi_1 - \phi_2) + \cos \alpha_2] \mathbf{e}_y \\ &\quad + [\sin \alpha_1 \cos(\phi_1 - \phi_2) - \sin \alpha_2] \mathbf{e}_x \}, \end{aligned} \quad (\text{C11})$$

$$\begin{aligned} \mathbf{S}_4 &= \frac{S}{2} \{ [1 - \cos(\phi_1 - \phi_2)] \mathbf{e}_z + \cos \alpha_1 \sin(\phi_1 - \phi_2) \mathbf{e}_y \\ &\quad + \sin \alpha_1 \sin(\phi_1 - \phi_2) \mathbf{e}_x \}. \end{aligned} \quad (\text{C12})$$

Thus, we successfully described the spin structure of model 3 with the two wave vectors. Because the models 1 and 2 are the particular cases of model 3, they can also be expressed.

- [1] Y. Taguchi, Y. Oohara, H. Yoshizawa, N. Nagaosa, and Y. Tokura, *Science* **291**, 2573 (2001).
- [2] M. Fiebig, V. V. Pavlov, and R. V. Pisarev, *J. Opt. Soc. Am. B* **22**, 96 (2005).
- [3] M. Fiebig, D. Fröhlich, K. Kohn, S. Leute, T. Lottermoser, V. V. Pavlov, and R. V. Pisarev, *Phys. Rev. Lett.* **84**, 5620 (2000).
- [4] G. L. J. A. Rikken and E. Raupach, *Nature (London)* **390**, 493 (1997).
- [5] Y. Tokura and N. Nagaosa, *Nat. Commun.* **9**, 3740 (2018).
- [6] G. L. J. A. Rikken, J. Fölling, and P. Wyder, *Phys. Rev. Lett.* **87**, 236602 (2001).
- [7] T. Ideue, K. Hamamoto, S. Koshikawa, M. Ezawa, S. Shimizu, Y. Kaneko, Y. Tokura, N. Nagaosa, and Y. Iwasa, *Nat. Phys.* **13**, 578 (2017).
- [8] T. Yokouchi, N. Kanazawa, A. Kikkawa, D. Morikawa, K. Shibata, T. Arima, Y. Taguchi, F. Kagawa, and Y. Tokura, *Nat. Commun.* **8**, 866 (2017).
- [9] G. L. J. A. Rikken and N. Avarvari, *Phys. Rev. B* **99**, 245153 (2019).
- [10] R. Aoki, Y. Kousaka, and Y. Togawa, *Phys. Rev. Lett.* **122**, 057206 (2019).
- [11] N. Jiang, Y. Nii, H. Arisawa, E. Saitoh, and Y. Onose, *Nat. Commun.* **11**, 1601 (2020).
- [12] M. Mekata, T. Sugino, A. Oohara, Y. Oohara, and H. Yoshizawa, *Physica B: Condens. Matter* **213-214**, 221 (1995).
- [13] H. Takatsu, G. Nénert, H. Kadowaki, H. Yoshizawa, M. Enderle, S. Yonezawa, Y. Maeno, J. Kim, N. Tsuji, M. Takata, Y. Zhao, M. Green, and C. Broholm, *Phys. Rev. B* **89**, 104408 (2014).
- [14] H. Takatsu, S. Yonezawa, S. Fujimoto, and Y. Maeno, *Phys. Rev. Lett.* **105**, 137201 (2010).
- [15] J. M. Ok, Y. J. Jo, K. Kim, T. Shishidou, E. S. Choi, H.-J. Noh, T. Oguchi, B. I. Min, and J. S. Kim, *Phys. Rev. Lett.* **111**, 176405 (2013).
- [16] H.-J. Noh, J. Jeong, B. Chang, D. Jeong, H. S. Moon, E.-J. Cho, J. M. Ok, J. S. Kim, K. Kim, B. I. Min, H.-K. Lee, J.-Y. Kim, B.-G. Park, H.-D. Kim, and S. Lee, *Sci. Rep.* **4**, 3680 (2014).
- [17] H. Takatsu and Y. Maeno, *J. Cryst. Growth* **312**, 3461 (2010).
- [18] P. J. Moll, *Annu. Rev. Condens. Matter Phys.* **9**, 147 (2018).
- [19] N. Ashcroft and N. Mermin, *Solid State Physics* (Saunders College Publishing, Philadelphia, 1976).
- [20] H. Murakawa, Y. Onose, F. Kagawa, S. Ishiwata, Y. Kaneko, and Y. Tokura, *Phys. Rev. Lett.* **101**, 197207 (2008).
- [21] H. Murakawa, Y. Onose, K. Ohgushi, S. Ishiwata, and Y. Tokura, *J. Phys. Soc. Jpn.* **77**, 043709 (2008).
- [22] D. Sun, D. A. Sokolov, J. M. Bartlett, J. Sannigrahi, S. Khim, P. Kushwaha, D. D. Khalyavin, P. Manuel, A. S. Gibbs, H. Takagi, A. P. Mackenzie, and C. W. Hicks, *Phys. Rev. B* **100**, 094414 (2019).
- [23] M. D. Le, S. Jeon, A. I. Kolesnikov, D. J. Voneshen, A. S. Gibbs, J. S. Kim, J. Jeong, H.-J. Noh, C. Park, J. Yu, T. G. Perring, and J.-G. Park, *Phys. Rev. B* **98**, 024429 (2018).
- [24] V. I. Fedorov, A. G. Gukasov, V. Kozlov, S. V. Maleyev, V. P. Plakhty, and I. A. Zobjkalo, *Phys. Lett. A* **224**, 372 (1997).
- [25] R. R. Birss, *Symmetry and Magnetism, in Selected Topics in Solid State Physics*, edited by E. P. Wohlfarth, Vol. 3 (North-Holland, Amsterdam, 1966).